

# X-ray Emissions from Three-dimensional Magnetohydrodynamic Coronal Accretion Flows

Norita KAWANAKA,<sup>1</sup> Yoshiaki KATO,<sup>2</sup> and Shin MINESHIGE<sup>1</sup>

<sup>1</sup>*Yukawa Institute for Theoretical Physics, Kyoto University, Kyoto 606-8502, Japan*

<sup>2</sup>*Center for Computational Sciences, University of Tsukuba 1-1-1 Tennodai, Tsukuba, Ibaraki*

*305-8511, Japan*

*norita@yukawa.kyoto-u.ac.jp*

(Received ; accepted )

## Abstract

We calculate the radiation spectrum and its time variability of the black hole accretion disk-corona system based on the three-dimensional magnetohydrodynamic simulation. In explaining the spectral properties of active galactic nuclei (AGNs), it is often assumed that they consist of a geometrically thin, optically thick disk and hot, optically thin corona surrounding the thin disk. As for a model of the corona, we adopt the simulation data of three-dimensional, non-radiative MHD accretion flows calculated by Kato and coworkers, while for a thin disk we assume a standard type disk. We perform Monte Carlo radiative transfer simulations in the corona, taking into account the Compton scattering of soft photons from the thin disk by hot thermal electrons and coronal irradiation heating of the thin disk, which emits blackbody radiation. By adjusting the density parameter of the MHD coronal flow, we can produce the emergent spectra which are consistent with those of typical Seyfert galaxies. Moreover, we find rapid time variability in X-ray emission spectra, originating from the density fluctuation produced by the magnetorotational instability in the MHD corona. The features of reflection component including iron fluorescent line emission are also briefly discussed.

**Key words:** accretion, accretion disks — black hole physics — radiative transfer  
– X-rays: general

## 1. Introduction

Thanks to the rapid progress in the observational studies in recent years, our understanding of the radiation properties of black hole accretion flows have been really deepened. Accreting black holes, such as active galactic nuclei (AGNs) and black hole binaries (BHBs) dur-

ing their very-high spectral state [state with luminosities around a few tenths of the Eddington limit ( $L_{\text{Edd}}$ )], show the radiation spectra dominated by two components; the thermal bump in UV/soft X-ray band and the power-law emission with a spectral index of  $\alpha \sim 1$  in the X-ray band (possibly with a high energy cutoff around MeV; for the multiwavelength spectrum of a typical AGN, see Reynolds et al. 1997). These components are often explained by the disk-corona model (Liang & Price 1975; Bisnovatyi-Kogan & Blinnikov 1977; Haardt & Maraschi 1991, 1993). In this model, the accretion flow consists of geometrically thin, optically thick accretion disk whose structure is studied by Shakura & Sunyaev (1973), and hot, optically thin corona surrounding the disk. The thermal bump is believed as the thermal emission from the optically thick disk (see Kishimoto et al. 2005 for its observational implication), and the power-law component is interpreted to be formed by photons which are emitted from the disk and Compton up-scattered by hot electrons in the corona (see Thorne & Price 1975; Shapiro et al. 1976 but in the context of the inner hot accretion flow model). Such a structure that the hot gas (i.e. the corona) coexists with the cool gas (i.e. the disk) is justified by the existence of the reflection component observed in the X-ray spectra (Pounds et al. 1990; see also Guilbert & Rees 1988; Lightman and White 1988). This reflection component is accompanied by the iron fluorescent line emission broadened relativistically (for reviews, see Mushotzky et al. 1993; Fabian et al. 2000; Reynolds & Nowak 2003).

On the other hand, our theoretical understanding of black hole accretion has also made a rapid progress. Now the dynamics of accretion flows is understood in terms of magnetohydrodynamics (MHD), since Balbus & Hawley (1991) rediscovered the magnetorotational instability (MRI) as the fundamental mechanism of angular momentum transfer in accretion disks. Detailed dynamical features of MHD accretion flows have been investigated via global three-dimensional numerical simulations (Matsumoto 1999; Stone & Pringle 2001; Machida et al. 2001; Hawley & Krolik 2001, 2002; Machida & Matsumoto 2003; Armitage & Reynolds 2003; De Villiers et al. 2003; Gammie et al. 2003; Igumenshchev et al. 2003). Such magnetically dominated accretion flows as those simulated in these calculations are radiatively inefficient accretion flows (RIAFs) whose mass accretion rates are much smaller than the critical value of  $\sim L_{\text{Edd}}$  (see, e.g., Mineshige et al. 1995). In such flows, the dissipated energy would not be radiated away efficiently, because of their low density, and be advected inward to the central black hole (Ichimaru 1977; Narayan & Yi 1994; Abramowicz et al. 1995; Kato et al. 1998).

Although the detailed structures and behavior of magnetohydrodynamical accretion flows are shown by numerical methods, it is still unclear that if these simulational results can be applied in realistic situations in the universe. In recent years, the researches concerning the observational properties like the spectra and their time variabilities expected from numerically simulated accretion flows have been extensively performed. Since the RIAF model is believed to fit the emergent spectrum of Sagittarius A\*, some authors have calculated the time dependent radiation spectra predicted from simulated MHD accretion flows with the aim to reproduce

the observed behavior of Sgr A\* (Hawley & Balbus 2002; Goldstone et al. 2005; Ohsuga et al. 2005; Moscibrodzka et al. 2007). However, as for the accretion flows with moderately high mass accretion rate, which are considered to be a good model for AGNs and BHBs showing the thermal bump and the power-law emission in their spectra, no attempts have been made so far to calculate the spectra predicted from MHD simulations taking into account realistic radiation processes. As noted in the above, in order to reproduce such spectra, the simulated accretion flows should have two components: geometrically thin cool disk and optically thin hot corona. However, no simulation data which incorporate such two-component effects are available.

In this study we calculate for the first time the emergent spectra of two-component accretion flows based on the three-dimensional MHD simulation by Kato et al. (2004, hereafter KMS04). Instead of fully solving the dynamics of two-component accretion flows, we adopt the simulation result of RIAF-like MHD accretion flow for the optically thin corona, and assume that the optically thick, geometrically thin disk is embedded in the corona with mutual interaction through radiation. Other interactions, such as mass evaporation/condensation or heat conduction, are neglected, for simplicity (Meyer & Meyer-Hofmeister 1994; Meyer et al. 2000; Liu et al. 2002, 2007). The disk is emitting soft photons with thermal spectrum, and those photons are up-scattered by hot electrons in the corona. After being scattered in the corona, a part of upscattered photons return to the disk and are thermalized there, thereby heating the accretion disk. The disk emission is, hence, enhanced by this returning process. In this paper we perform three-dimensional Monte Carlo radiative transfer simulations to properly calculate such radiation processes and the emergent spectra.

The plan of this paper is as follows. We show the detail of the model and method used in our calculation in §2. The results are presented in §3, and compare them with the spectra observed in typical AGNs and discuss the similar points and discrepancies between them in §4. In §5 we summarize our study.

## 2. MODEL AND CALCULATION METHODS

### 2.1. Overview of Adopted MHD Simulations

KMS04 investigated the evolution of a torus threaded by weak localized poloidal magnetic fields by performing the three-dimensional MHD simulation. They solved the following basic equations of the resistive MHD in the cylindrical coordinates,  $(r, \phi, z)$ :

$$\frac{\partial \rho}{\partial t} + \nabla \cdot (\rho \mathbf{v}) = 0, \quad (1)$$

$$\frac{\partial}{\partial t}(\rho \mathbf{v}) + \nabla \cdot \left( \rho \mathbf{v} \otimes \mathbf{v} - \frac{\mathbf{B} \otimes \mathbf{B}}{4\pi} \right) = -\nabla \left( p_{\text{gas}} + \frac{B^2}{8\pi} \right) - \rho \nabla \psi, \quad (2)$$

$$\frac{\partial}{\partial t} \left( \varepsilon + \frac{B^2}{8\pi} \right) + \nabla \cdot \left[ (\varepsilon + p_{\text{gas}}) \mathbf{v} + \frac{c(\mathbf{E} \times \mathbf{B})}{4\pi} \right] = -\rho \mathbf{v} \cdot \nabla \psi, \quad (3)$$

$$\frac{\partial B}{\partial t} = -c \nabla \times \mathbf{E}, \quad (4)$$

where  $\psi = -GM/(R - r_S)$  is the pseudo-Newtonian potential (Paczynski & Wiita 1980),  $\varepsilon = \rho v^2/2 + p_{\text{gas}}/(\gamma - 1)$  is the energy of the gas (here  $\gamma$  is fixed to be 5/3) and  $\mathbf{E} = -(\mathbf{v}/c) \times \mathbf{B} + (4\pi\eta/c^2)\mathbf{J}$  is Ohm's law. Here  $R [\equiv (r^2 + z^2)^{1/2}]$  is the distance from the origin,  $r_S (\equiv 2GM/c^2)$  is the Schwarzschild radius (with  $M$  and  $c$  being the mass of a BH and the speed of light, respectively), and  $\mathbf{J} = (c/4\pi)\nabla \times \mathbf{B}$  is the electric current. As to  $\eta$  we adopt the anomalous resistivity model which is used in many solar flare simulations (for the detail, see Yokoyama & Shibata 1994). The calculation is started with a rotating torus in hydrostatic balance located around  $r = r_0 = 40r_S$ . The initial magnetic fields are confined within a torus and purely poloidal (see KMS04 for the detail). In the simulation they used  $300 \times 32 \times 400$  nonuniform mesh points. The grid spacing is uniform ( $\Delta r = \Delta z = 0.16r_S$ ) within the inner calculation box of  $0 \leq z \leq 10r_S$ , and it increases by 1.5% from one mesh to the adjacent outer mesh outside this box up to  $r \leq 20r_S$  and  $z \leq 20r_S$ , and it increases by 3% beyond that. The entire computational box size is  $0 \leq r \leq 200r_S$ ,  $0 \leq \phi \leq 2\pi$ , and  $-50r_S \leq z \leq 50r_S$ , and they simulated a full  $360^\circ$  domain (see Kato 2004 for more detail).

The simulated MHD flow is slightly oscillating because of the turbulence driven by MRI, and geometrically thick density distribution is produced. In this quasi-steady accretion flow, the density profile is  $\rho \propto r$  in the inner part ( $r < 20r_S$ ), while  $\rho \propto r^{-1}$  in the outer part ( $r > 20r_S$ ) (see Fig. 4 in KMS04). We use this quasi-steady density distribution as well as the ion temperature distribution in modeling the corona in which hot thermal electrons up-scatter the soft photons emerging from the cold disk virtually located in the equatorial plane.

## 2.2. Physical Quantities of the Disk and Corona

As mentioned in §1 briefly, we adopt the following assumptions in constructing the disk-corona model.

1. In the equatorial plane, we assume a standard accretion disk (Shakura & Sunyaev 1973) with an infinitesimal height for a given mass accretion rate  $\dot{M}_{\text{disk}}$ .
2. The RIAF-like accretion flow, whose structure is provided by the three-dimensional MHD simulation (KMS04), is surrounding the standard thin disk as the hot corona. That is, we assume that coronal flow is created at large radius by evaporation of the disk material and moves freely inward<sup>1</sup>. Mass evaporation and condensation occurring between them and heat conduction from the corona to the disk are neglected in the calculation. Radiative cooling of coronal plasma is also neglected.
3. The photons radiated from the thin disk are partly up-scattered by hot electrons in the corona and the remaining portion penetrate through the corona, creating a power-law hard emission in the spectrum.

---

<sup>1</sup> Note that evaporation dominates over condensation at large radii, whereas the opposite is the case at small radii (e.g. Liu et al. 2007)

4. As the seed photon field from the underlying disk, we include the reprocessed radiation, which comes from the coronal irradiation on the disk, as well as the intrinsic disk radiation.

We take three-dimensional data of density and proton temperature distributions in the accretion flows calculated in Kato (2004). This has the same initial condition with Model B in KMS04. The data of physical properties are given at each point in the simulation box associated with Cartesian coordinates  $(x, y, z)$ , in which the black hole is located at the origin of the coordinate axes, the  $z$ -axis is set to be the rotation axis of the accretion flow, and the  $x$ - $y$  plane corresponds to the equatorial plane. We employ Cartesian grids with numbers  $(N_x, N_y, N_z) = (101, 101, 101)$  of cells. The size of the calculating box is  $2X \times 2Y \times 2Z$ , where we set  $(X, Y, Z) = (99.9r_S, 99.9r_S, 99.9r_S)$ .

In the MHD simulations with no radiative loss the density is given as non-dimensional number  $\tilde{\rho}$  with the normalization factor  $\rho_0$ , which is treated a free parameter in our calculation. Basically the coronal density is determined by evaporation of the disk gas, but here we determine  $\rho_0$  so that the power-law indices of the evaluated spectra agree with the observations. The proton temperature does not depend on the density parameter and is given by the MHD simulation as  $(\mu m_p c^2 / k_B) \tilde{c}_s^2$ , where  $\mu$  is the mean molecular weight ( $= 0.5$ ),  $m_p$  is the proton mass,  $k_B$  is the Boltzmann constant, and  $\tilde{c}_s$  is the normalized sound velocity obtained by the simulation.

Here we should note that ions (protons) and electrons in the plasma simulated in KMS04 have the same temperature, though electrons would be radiatively cooled and have lower temperature in the realistic situation. Assuming that ion temperature coincides with the simulated one and that the electrons have a Maxwellian distribution, we evaluate the electron temperature,  $T_e$ , through the energy balance of the electrons between Coulomb collisions with ions and radiative cooling,

$$\int_{-Z}^Z \int_{r_{\text{in}}}^{r_{\text{out}}} \lambda_{ie} 2\pi r dr dz = \int L_C(\nu; r_{\text{in}} \leq r \leq r_{\text{out}}) d\nu. \quad (5)$$

Here  $\lambda_{ie}$  is the energy transfer rate from ions to electrons (Stepney & Guilbert 1983) and  $L_C(\nu)$  is the coronal luminosity at frequency  $\nu$ . In the present study, we divide the corona into three regions ( $0 \leq r \leq 10r_S$ ,  $10r_S < r \leq 30r_S$ , and  $30r_S < r$ ;  $(r_{\text{in}}, r_{\text{out}}) = (0, 10r_S)$ ,  $(10r_S, 30r_S)$  and  $(30r_S, \infty)$ ) for simplicity, and suppose that the electrons in the accretion flow in each region have the temperature which is independent of the radius  $r$  and the altitude  $z$ . The coronal luminosity,  $L_C$ , is obtained by Monte Carlo simulations (see next subsection) for a guess value of  $T_e$ . Since this  $T_e$  does not always satisfy Eq. (5), we should do some iterations to calculate the appropriate electron temperature and the emergent spectrum.

### 2.3. Radiative Transfer Simulations

Our model consists of a cold disk which produces blackbody radiation at each radius with temperature being determined from the standard model (Shakura & Sunyaev 1973):

$$T_{\text{disk}}^0 = \left[ \frac{3GM\dot{M}_{\text{disk}}}{8\pi r^3\sigma} \left( 1 - \sqrt{\frac{r}{r_{\text{in}}}} \right) \right]^{1/4}, \quad (6)$$

(as long as the reprocessed radiation is unimportant) where  $G$  is the gravitational constant,  $\dot{M}_{\text{disk}}$  is the mass accretion rate in the disk, and  $\sigma$  is the Stephan-Boltzmann constant. Note that when irradiation flux  $F_{\text{irr}}$  by the corona is available, the disk emits blackbody with an enhanced temperature

$$T_{\text{disk}} = \left[ (T_{\text{disk}}^0)^4 + F_{\text{irr}}/\sigma \right]^{1/4}. \quad (7)$$

In the following calculation we set  $r_{\text{in}} = 3r_{\text{S}}$ ,  $\dot{M}_{\text{disk}} = 10^{-3}\dot{M}_{\text{Edd}}$  (with  $\dot{M}_{\text{Edd}} = 10L_{\text{Edd}}/c^2$ ) and the mass of a central black hole to be  $M = 10^8M_{\odot}$ , which is believed to be the typical value for AGNs. Thus, the normalized time corresponds to  $\tilde{t} \cong r_{\text{S}}/c = 10^3\text{sec}$ .

As the radiation process, we take into account both of the intrinsic disk radiation [Eq.(6)] and the thermal reprocessing from irradiated disk as the seed photon field [see Eq. (7)], and the Compton/inverse Compton scattering in the corona. We neglect synchrotron emission/absorption and free-free emission/absorption. Some studies about the disk-corona model have shown that the power-law component of the emergent spectra is explained as the Comptonized emission (Haardt & Maraschi 1991, 1993), so for our present purpose this approximation is justified at least in the X-ray energy bands. According to the simulation by KMS04, the magnetic field in the coronal flow with  $\rho_0 = 1.6 \times 10^{-14} \text{ g cm}^{-3}$  is  $B \sim 10^3\text{G}$ , for which the Compton scattering is the most efficient cooling mechanism. This fact justifies the method of deriving the coronal temperature described in the previous section.

The method of the Monte Carlo simulation is based on Pozdnyakov et al. (1977). In order to efficiently calculate the emergent spectra, we introduce a photon weight  $w$ . When emerged from the disk we set that each photon has the weight of  $w_0 = 1$ , and then we calculate the escape probability,  $P_0$ . The escape probability of a photon after  $i$ -th scattering (for  $i \geq 1$ ),  $P_i$ , is evaluated as

$$P_i = \exp \left( - \int \left[ \frac{\rho(x_i, y_i, z_i)}{m_p} \right] \sigma_{\text{KN}}(x_i, y_i, z_i) dl \right), \quad (8)$$

where  $(x, y, z) = (x_0, y_0, 0)$  corresponds to the point on the equatorial plane (i.e. the disk plane), in which the thermal soft photons are generated,  $(x_i, y_i, z_i)$  is the point where a photon is subject to the  $i$ -th scattering,  $m_p$  is the proton mass,  $\sigma_{\text{KN}}$  is the Klein-Nishina cross section (Rybicki & Lightman 1979), and the integral of  $dl$  should be done along the photon direction there from the point  $(x_i, y_i, z_i)$  to the boundary of the calculating box. The quantity of  $w_0P_0$  represents the transmitted portion of photons and is recorded to calculate the penetrated

spectrum if the path of the photon does not cross with the equatorial plane, and will no longer continue to be counted and will be regarded to be absorbed by the disk. As for the remaining portion of a photon, its weight becomes  $w_1 = w_0(1 - P_0)$ . The transmitted portion of photons after  $i$ -th scattering,  $w_i P_i$  is recorded to calculate the emergent spectrum, and the remaining portion,  $w_i(1 - P_i)$ , undergoes the  $(i + 1)$ -th scattering. This calculation is continued until the weight  $w_i$  becomes sufficiently small ( $w_i \ll 1$ ) or the path of the remaining photon crosses the equatorial plane, regarding to be absorbed by the disk. The whole process is simulated by the Monte Carlo method. Finally, we suppose that the inner boundary of the underlying standard disk is  $r = 3r_S$ , and general relativistic effects like the light bending and energy shift are neglected in our study.

### 3. Results

#### 3.1. Spectral Features

First, we show the emergent spectra from the accretion disk with MHD coronal flow with various density parameters for the corona in Fig. 1. In this calculation, the mass accretion rate of the underlying disk is set to be  $\dot{M}_{\text{disk}} = 10^{-3} M_{\text{Edd}}$ . This value is relatively lower than that assumed in the standard picture ( $\dot{M}_{\text{disk}} \sim 0.1 - 0.01 M_{\text{Edd}}$ ). However, according to the idea of Haardt & Maraschi (1991), the liberated gravitational energy accompanying the mass accretion  $L_G$  should be mostly dissipated in the corona ( $f L_G$ , where  $f \simeq 1$ ), while only a small fraction of the energy ( $(1 - f)L_G$ ) is dissipated in the underlying disk. Then the temperature of the intrinsic disk radiation would be reduced by a factor of  $(1 - f)^{1/4}$ . In our calculation the mass accretion rate of the disk only appears when giving the intrinsic disk temperature Eq. (6), and so the small mass accretion rate corresponds to the reduced disk temperature. Due to this fact, the relatively small mass accretion rate adopted in our calculation is justified.

The adopted density parameters  $\rho_0$  for the corona are  $\rho_0 = 5.1 \times 10^{-15}$ ,  $1.6 \times 10^{-14}$ , and  $5.1 \times 10^{-14} \text{ g cm}^{-3}$ . These values correspond to the number density of  $\sim 10^9 \text{ cm}^{-3}$ . Such density is consistent with some corona models (see Liu et al. 2002, 2003). Due to the inverse Compton scattering of in which the soft thermal photons from the underlying disk in the corona, the power-law component with the spectral index of  $\alpha \sim 1 - 2$  ( $F_\nu \propto \nu^{-\alpha}$ ) appears in the higher energy band. In the calculated spectra, we cannot find a bump-like structure clearly in the UV/soft X-ray band which is usually seen in typical spectra of AGNs. As  $\rho_0$  increases, the total luminosities increases, while the power-law index decreases. The corona with higher density (especially with higher scattering optical depth) would irradiate the underlying disk with higher energy flux because larger number of photons originated from the disk would gain the energy and be backscattered. The the disk is heated by the corona and so the energy flux of the seed photon field would increase. This is why the total luminosity rises with the coronal density.

In Table 1 we summarize the scattering optical depths  $\tau$  (evaluated by integrating the

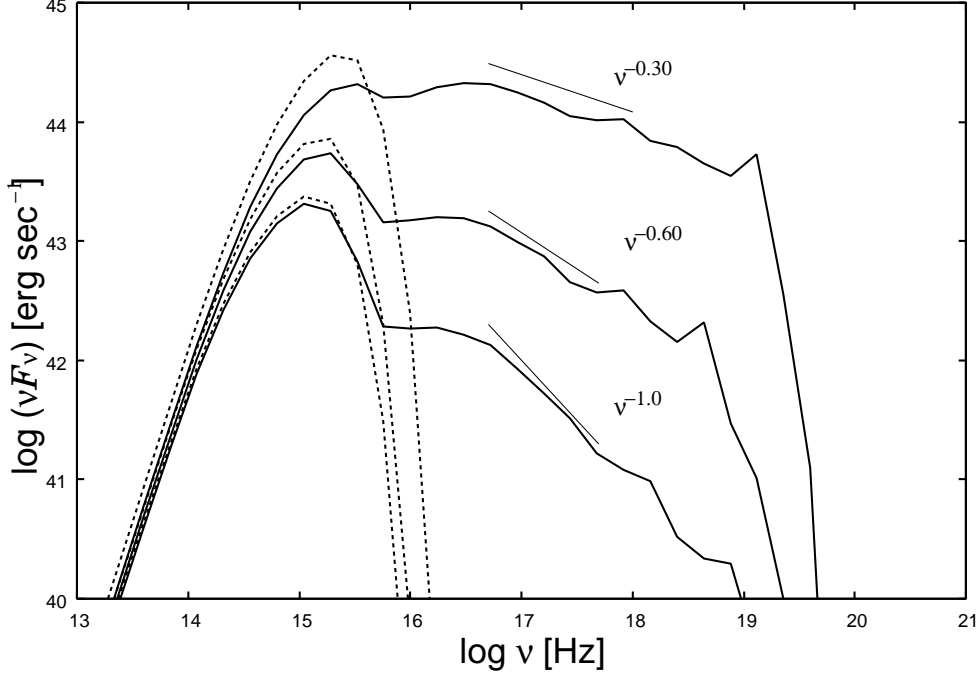


**Fig. 1.** Broadband spectra from a disk at the accretion rate of  $10^{-3}\dot{M}_{\text{Edd}}$  and a MHD coronal flow around a black hole of  $10^8 M_{\odot}$  with the density normalization parameters  $5.1 \times 10^{-15}$ ,  $1.6 \times 10^{-14}$  and  $5.1 \times 10^{-14} \text{ g cm}^{-3}$  *solid lines*. The spectra of the seed photons (including those from the cold disk and the reflection component; *dashed lines*) are also shown for the comparison. The short solid lines near the spectra show the power-law fit of  $\nu F_{\nu}$ .

**Table 1.** Coronal properties

$\rho_0 \text{ (g cm}^{-3}\text{)}$	region	$T_{\text{cor}} \text{ [K]}$	$\tau$	$y$	$\alpha$
$5.1 \times 10^{-14}$	$0 < r < 10r_{\text{S}}$	$\sim 5.2 \times 10^9$	$\sim 0.2$	$\sim 0.5$	$\sim 1.30$
	$10r_{\text{S}} < r < 30r_{\text{S}}$	$\sim 3.4 \times 10^9$	$\sim 0.9$	$\sim 3$	
	$30r_{\text{S}} < r$	$\sim 7.6 \times 10^8$	$\sim 0.7$	$\sim 0.5$	
$1.6 \times 10^{-14}$	$0 < r < 10r_{\text{S}}$	$\sim 5.2 \times 10^9$	$\sim 0.05$	$\sim 0.2$	$\sim 1.60$
	$10r_{\text{S}} < r < 30r_{\text{S}}$	$\sim 3.4 \times 10^9$	$\sim 0.25$	$\sim 0.55$	
	$30r_{\text{S}} < r$	$\sim 7.5 \times 10^8$	$\sim 0.2$	$\sim 0.1$	
$5.1 \times 10^{-15}$	$0 < r < 10r_{\text{S}}$	$\sim 5.2 \times 10^9$	$\sim 0.02$	$\sim 0.05$	$\sim 2.00$
	$10r_{\text{S}} < r < 30r_{\text{S}}$	$\sim 3.4 \times 10^9$	$\sim 0.09$	$\sim 0.15$	
	$30r_{\text{S}} < r$	$\sim 7.6 \times 10^8$	$\sim 0.07$	$\sim 0.03$	

scattering opacity over the z-direction from the equatorial plane), and the Compton  $y$  parameters of the corona (averaged in each region), and the spectral indices of the power law component estimated from the calculation results for 3 density parameters. The MHD simulation of coronal flow was started from the initial condition of a magnetized torus located around at  $r \sim 40r_{\text{S}}$ . The radius of maximum gas density (and of maximum  $\tau$ ) decreases inward with

time and stays around  $r \sim 20r_g$ . According to the theory of unsaturated inverse Compton scattering, the power-law index of the Comptonized emission component depends on the plasma density and temperature through this equation:

$$\alpha = -\frac{3}{2} + \sqrt{\frac{9}{4} + \frac{4}{y}}. \quad (9)$$

Here  $y \equiv (4k_B T/m_e c^2)\tau$  is the Compton  $y$ -parameter (Rybicki & Lightman 1973), where  $T$  and  $\tau$  are the temperature and Thompson optical depth of the corona, respectively. The spectral indices derived from this equation using  $y$ -parameters in Table 1 do not always agree with those estimated from the spectra. This is because  $\tau$  and  $T_{\text{cor}}$  have spatial distributions and we cannot evaluate  $y$ -parameter of the corona uniquely. Even with such a situation, however, we can see the tendency that the spectra get flatter with higher coronal density (and then higher  $y$ -parameter), which is consistent with the theory above.

In our calculation,  $\rho_0$  is determined so as to reproduce the observation. By tuning the coronal density parameter, we can reproduce the luminosity of the power-law component which is as intense as that of the thermal component originated from the optically thick disk. Such feature is typical in Seyfert galaxies. However, the coronal temperature cannot be chosen freely but should be determined by imposing the energy balance of the electrons between Coulomb collisions and the cooling via inverse Compton scattering, as we have done. Nevertheless the resulting coronal temperature is substantially reduced from the plasma temperature derived by the simulation ( $\sim 10^{13}$  K) to  $\sim 10^9$  K, which makes the high energy cutoff of computed spectra consistent with observations.

### 3.2. Time variation

The spectral variation caused by the time variation of MHD coronal flow structure is shown in Fig. 2. In the highest energy range ( $\gtrsim 10^{18}$  Hz) the spectra show fluctuations because of poor photon statistics. As for the soft X-ray band (with  $\log \nu \simeq 17 - 18$ ) where the spectra show a smooth power-law shape, the spectral index slightly changes with time, and then the X-ray flux fluctuates a little (see also Fig. 3). According to the MHD simulation on which our radiative transfer calculations are based, the three-dimensional structure of the coronal accretion flow is fluctuating everywhere in each timestep. On the other hand, the spectral index depends on the distribution of  $y$ -parameter of the corona, as we note in the last subsection. So we can conclude that the fluctuations of the spectral indices of the computed spectra in Fig. 2 reflect the fluctuation of  $y$ , which comes from the density fluctuations (which is supposed to be due to MRI) in the coronal flow.

Fig. 3. shows the X-ray lightcurve derived from our simulations. From this plot we can see that the X-ray luminosity from our disk-corona system can change by factors of a few tens of percent on timescales of the orbital period at the last stable orbit ( $r = 3r_g$ ), i.e. about  $10^3(M/10^8)M_\odot$  sec. In the whole calculation we do not vary the properties of the soft photon

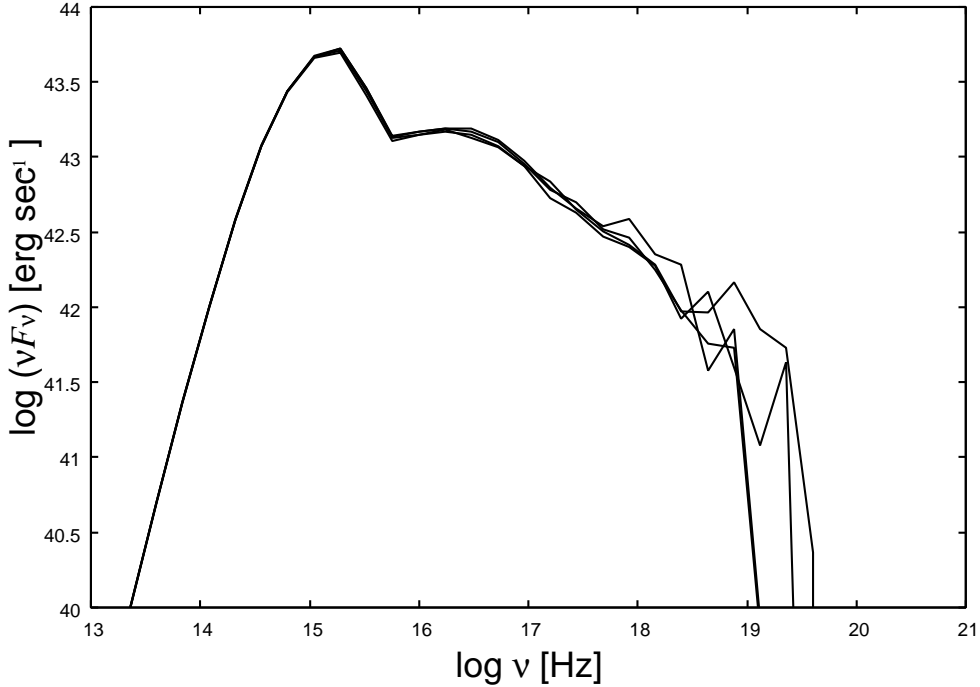


**Fig. 2.** Spectral variation of the Comptonized emission predicted from the standard disk with a MHD coronal flow around a black hole of  $10^8 M_\odot$ . Here we set the density parameter as  $1.6 \times 10^{-14} \text{g cm}^{-3}$ .

source (i.e. the underlying cold disk). This variation which we obtained is due to the density fluctuation (and accompanying temperature fluctuation) of the coronal flow.

#### 4. Discussion and Conclusion

We have calculated the emergent spectra and their time variabilities predicted based on the disk-corona model, in which a cold standard disk at the equatorial plane is sandwiched by a hot coronal flow. As for the structure and dynamics of the corona we use the three-dimensional MHD simulation data by Kato (2004). In this section we discuss our results especially in the context of AGNs.

We have shown that our black hole disk-corona system can reproduce the power-law X-ray emission with the photon index  $\alpha \sim 1 - 2$  by adjusting the density parameter properly. The power-law indices and the cutoff energy scales of the spectra are roughly in agreement with the observed spectra of Seyfert galaxies. Moreover, we find significant variability of the power-law X-ray emission. The power-law X-ray emission flux predicted from our model changes by a few tens of percent on timescales of the orbital period near the last stable orbit, which is about  $10^3 (M/10^8 M_\odot)$  sec, while the power-law index nor the cutoff energy do not change considerably. This variability comes purely from the fluctuation of the coronal flow around  $r \sim 20 r_S$ , where the scattering optical depth of the coronal flow attains its largest value in its structure. This fluctuation is driven by the turbulence as a result of MRI, and its amplitude is large enough

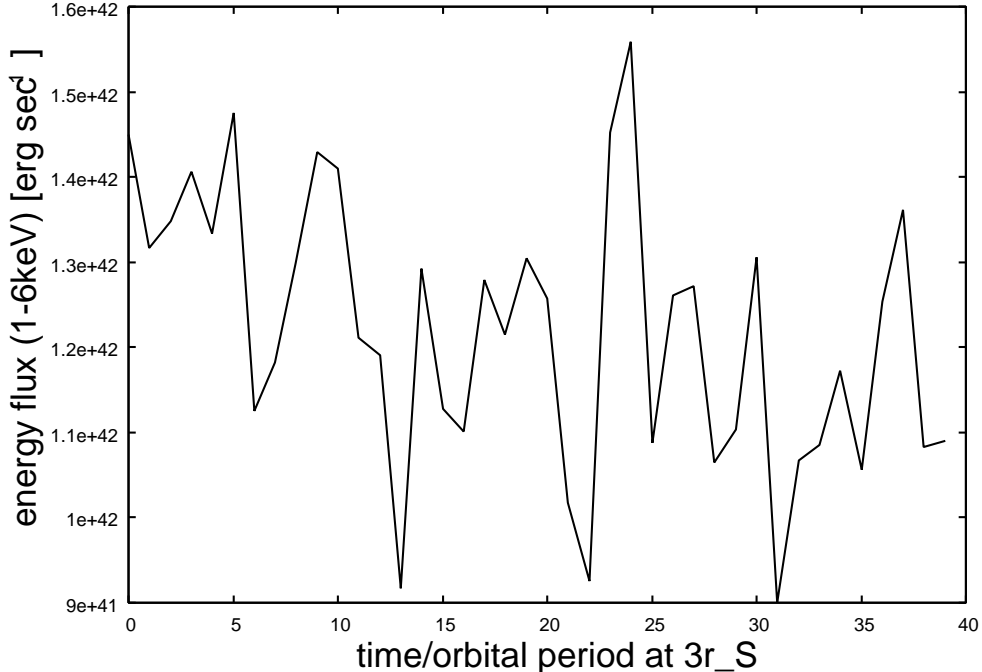


**Fig. 3.** Time variation of the X-ray luminosity (1-6keV). Here we set the density parameter as  $1.6 \times 10^{-14} \text{g cm}^{-3}$ .

to explain the observed X-ray variability in Seyfert galaxies (e.g. Miniutti et al. 2007). In UV/soft X-ray band, however, we cannot see the bump-like structure which is often found in the spectra of AGNs. The same problem occurred in other disk-corona models (Shimura et al. 1995; Liu et al. 2003). This bump is supposed to be the thermal radiation coming directly from the optically thick disk, while in those disk-corona models the disk is wholly covered with corona. In order to reproduce the UV/soft X-ray bump with a model, the coronal structure may need to be patchy or locally concentrated. In the present study we do not consider the viewing angle dependence of the spectra. If we observe this accretion flow system face-on, then the scattering optical depth along the line of sight would be smaller than in the case observed with non-zero viewing angle and the optically thick component should be observed more clearly.

Iron  $K\alpha$  fluorescent line emissions would occur when the disk is irradiated by X-ray from the corona. The profile of this line emission would be broadened due to relativistic effects (see Reynolds & Nowak 2003 for a review). The detailed structure of this line profile is determined by the line emissivity distribution on the disk, which depends on the spectra of local X-ray irradiation from the corona.

Recently *Suzaku* has observed the broadened iron line profile from MCG-6-30-15 in detail and they implied that the emissivity profile should be as steep as  $F_{\text{line}}(r) \propto r^{-4.4}$  (Miniutti et al. 2007). This is not easy to understand, since standard disks are known to produce continuum flux  $F_{\text{cont}}(r) \propto r^{-3}$ . Some authors proposed that this is a manifestation of Kerr black hole effects (e.g. Wilms et al. 2001). Such a steep emissivity profile can be reproduced by thermal

Comptonization in the corona, if the irradiating corona has the temperature and density profiles which are arising inward, as was pointed out by Kawanaka et al. (2005). This is because the fraction of high energy photons increases inward so that the number of irradiating photons which are capable of producing iron fluorescent line emissions should increase inward more rapidly than  $r^{-3}$ . As for the MHD corona model which we adopted in this study, however, the temperature and density have flatter profiles (see KMS04), so such a steep line emissivity profile is not expected as long as we consider only Compton upscattering to be the X-ray emission process in this corona.

One of the way of producing such a steep emissivity profile so as to produces the iron line profile as is observed is to introduce moderate radiative cooling in the simulation (Mineshige et al. 2002). Radiative cooling can be efficient in dense region which is generally located in the inner part of the disk. Then the density profile near the event horizon of the coronal flow can be steeper and Compton up-scattering would be more efficient. As a result, hard X-ray photons irradiating the disk would increase and iron fluorescence line photons would become more efficient. Another possibility is that the transient X-ray emission accompanying with magnetic reconnection flares in the localized region of the corona would contribute to the iron line emissions from the disk, which is not taken into account in our present calculation. Such small-scale X-ray sources are often assumed when explaining the constant reflection component including iron line emissions (Miniutti & Fabian 2004; Malzac et al. 2006; Nayakshin 2007). If we analyze the local electron heating (or nonthermal acceleration) around magnetic reconnection flares and hard X-ray emission processes in the MHD coronal flow simulation, then we can know the local X-ray irradiation onto the disk, which may lead us to understanding the observed broad iron line profiles and their time variabilities from the microphysics of X-ray emission processes.

We can check the consistency of the assumption that the MHD coronal flow which we adopt in the calculation is cooled dominantly by advection, by comparing the heating rate ( $\sim GMm_p/(2r)\Omega$ ) and the cooling rate ( $\sim$ Comptonization luminosity per electron). According to the result of our calculation, the innermost region ( $0 < r \lesssim 20r_S$ ) is not cooled efficiently by inverse Compton scattering. However, in the outer region ( $r \gtrsim 20r_S$ ) local heating rate and cooling rate are comparable, which means that the assumption of an advection-dominated flow is only marginally justified. Generally when Compton cooling becomes efficient the coronal temperature will become lower, and then Compton upscattering will be inefficient. This means that the power-law X-ray emission would not be generated so much from that region. As far as we consider the spectrum and energy flux in X-ray and higher energy band, to which the photons from the innermost region mainly contribute, this inconsistency would hardly affect the results.

Finally, we should mention the interaction between the corona and the underlying disk. In the transition zone between the hot corona and the cold disk where density and temperature

abruptly change, the heat conduction and the mass evaporation would be important as the mass and energy exchanging processes (Meyer & Meyer-Hofmeister 1994; Liu et al. 2002). Evaporation of photospheric material was actually shown to be essential in the context of solar flares (see e.g. Yokoyama & Shibata 1994). By including these effects in the simulation we will be able to obtain a more realistic model of the coronal structure and dynamics. To what extent the disk-corona structure can extend to the inner region is important when we consider the relativistic skewing of the iron line emission profile because most of the observations of iron line profiles imply that the iron fluorescence line photons are emitted from around/inside the last stable orbit. The detailed analysis of such disk-corona interactions and their observational implications are left as a future work.

We would like to thank Masayuki Umemura, Toshihiro Kawaguchi and Ken Ohsuga for helpful comments and discussions. We are also grateful to an anonymous referee for his/her valuable comments, which helped us to improve the manuscript in a great deal. The numerical calculations were carried out on Altix3700 BX2 at YITP in Kyoto University. This work is supported in part by Research Fellowship of the Japan Society for the Promotion of Science for Young Scientists (N. K.).

## References

- Abramowicz, M. A., Chen, X., Kato, S., Lasota, J.-P & Regev, O. 1995, *ApJ*, 438, L37  
Armitage, P. J. & Reynolds, C. S. 2003, *MNRAS*, 341, 1041  
Balbus, S. A. & Hawley, J. F. 1991, *ApJ*, 376, 214  
Bisnovatyi-Kogan, G. S. & Blinnikov, S. I. 1977, *A&A*, 59, 111  
De Villiers, J. -P., Hawley, J. F. & Krolik, J. H. 2003, *ApJ*, 599, 1238  
Fabian, A. C., Iwasawa, K., Reynolds, C. S., Young, A. J., 2000, *PASP*, 112, 1145  
Gammie, C. F., McKinney, J. C. & Toth, G. 2003, *ApJ*, 589, 444  
Goldston, J. E., Quataert, E. & Igumenshchev, I. V. 2005, *ApJ*, 621, 785  
Guilbert, P. W. & Rees, M. J. 1988, *MNRAS*, 233, 475  
Haardt, F. & Maraschi, L. 1991, *ApJ*, 380, L51  
Haardt, F. & Maraschi, L. 1993, *ApJ*, 413, 507  
Hawley, J. F. & Krolik, J. H. 2001, *ApJ*, 548, 348  
Hawley, J. F. & Krolik, J. H. 2002, *ApJ*, 566, 164  
Ichimaru, S. 1977, *ApJ*, 214, 840  
Igumenshchev, I. V., Narayan, R. & Abramowicz, M. A. 2003, *ApJ*, 592, 1042  
Kato, S., Fukue, J. & Mineshige, S. 1998, *Black-Hole Accretion Disks* (Kyoto: Kyoto Univ. Press)  
Kato, Y. 2004, *PASJ*, 56, 931  
Kato, Y., Mineshige, S. & Shibata, K. 2004, *ApJ*, 605, 307 (KMS04)  
Kawanaka, N., Mineshige, S. & Iwasawa, K. 2005, *ApJ*, 635, 167  
Kishimoto, M., Antonucci, R., & Blaes, O. 2005, *MNRAS*, 364, 640

Liang, E. P. T & Price, R. H. 1988, ApJ, 218, 247  
 Lightman, A. P. & White, T. R. 1988, ApJ, 335, 57  
 Liu, B. F., Mineshige, S., Meyer, F., Meyer-Hofmeister, E. & Kawaguchi, T. 2002, ApJ, 575, 117  
 Liu, B. F., Taam, R. E., Meyer-Hofmeister, E. & Meyer, F. 2007, arXiv:0709.0143, ApJ accepted  
 Machida, M. & Matsumoto, R. 2003, ApJ, 585, 429  
 Machida, M., Matsumoto, R. & Mineshige, S. 2001, PASJ, 53, L1  
 Malzac, J., Merloni, A. & Suebsuwong, T. 2006, Astron. Nachr., 327, 985  
 Matsumoto, R. 1999, in Numerical Astrophysics, ed. S. M. Miyama, K. Tomisaka & T. Hanawa  
 (Boston: Kluwer), 195  
 Meyer, F., Liu, B. F. & Meyer-Hofmeister, E. 2000, A&A, 361, 175  
 Meyer, F. & Meyer-Hofmeister, E. 1994, A&A, 288, 175  
 Mineshige, S., Negoro, H., Matsumoto, R., Machida, M. & Manmoto, T. 2002, in Current High Energy  
 Emission around Black Holes, ed. C. -H. Lee & H. -Y. Chang (Singapore: World Scientific), 119  
 Miniutti, G. & Fabian, A. C. 2004, MNRAS, 349, 1435  
 Miniutti, G. et al. 2007, PASJ, 59, 315  
 Moscibrodzka, M., Proga, D., Czerny, B. & Siemiginowska, A. 2007, arXiv:0707.1403  
 Mushotzky, R. F., Done, C. & Pounds, K. A. ARA&A, 31, 717  
 Narayan, R. & Yi, I. 1994, ApJ, 428, L13  
 Nayakshin, S. 2007, MNRAS, 376, L25  
 Ohsuga, K., Kato, Y. & Mineshige, S. 2005, ApJ, 627, 782  
 Pounds, K. A., Nandra, K., Stewart, G. C., George, I. M. & Fabian, A. C. 1990, Nature, 344, 132  
 Pozdnyakov, L. A., Sobol, I. M. & Sunyaev, R.A. 1977, Soviet Astron., 21, 708  
 Reynolds, C. S., Ward, M. J., Fabian, A. C. & Celotti, A. 1997, MNRAS, 291, 403  
 Reynolds, C. S. & Nowak, M. A. 2003, Phys. Rep., 377, 389  
 Rybicki, G. B., & Lightman, A. P. 1979, Radiative Processes in Astrophysics (New York: Wiley)  
 Shakura, N. I. & Sunyaev, R. A. 1973, A&A, 24, 337  
 Shapiro, S. L., Lightman, A. P. & Eardley, D. M. 1976, ApJ, 204, 187  
 Shimura, T., Mineshige, S. & Takahara, F. 1995, ApJ, 439, 74  
 Stone, J. M. & Pringle, J. E. 2001, MNRAS, 322, 461  
 Thorne, K. S. & Price, R. H. 1975, ApJ, 195, L101  
 Wilms, J., Reynolds, C. S., Begelman, M. C., Reeves, J., Molendi, S., Staubert, R. & Kendziorra, E.  
 2001, MNRAS, 328, L27  
 Yokoyama T. & Shibata, K. 1994, ApJ, 436, L197